Proceedings of the ASME 2010 3rd Joint US-European Fluids Engineering Summer Meeting and 8th International Conference on Nanochannels, Microchannels, and Minichannels
FEDSM-ICNMM2010
August 1-5, 2010, Montreal, Canada

FEDSM-ICNMM2010-30658

THE JETTING BEHAVIOR FROM SINGLE LASER INDUCED BUBBLES GENERATED ABOVE A SOLID BOUNDARY WITH A THROUGH HOLE

Jack E Abboud
Department of Mechanical Engineering
American University of Beirut
PO Box 11-0236, Beirut 1107-2020, Lebanon

Ghanem F Oweis
Department of Mechanical Engineering
American University of Beirut
PO Box 11-0236, Beirut 1107-2020, Lebanon
(goweis@aub.edu.lb)

ABSTRACT

An inertial bubble collapsing near a solid boundary generates a fast impulsive micro jet directed towards the boundary. The jet impact on the solid boundary can cause pitting, and this effect has been taken advantage of in surgeries such as when micro-bubbles are driven ultrasonically to cavitate in tissue and produce jets that are believed to induce the surgical effect. In this experimental investigation we are interested in the jetting from single cavitation bubbles near boundaries. By introducing a through hole in the boundary beneath a single laser-induced bubble it is hypothesized that the forming jet upon bubble implosion will proceed to penetrate through the hole to the other side and that it may be utilized in useful application such as precise surgeries. We study the cases of a bubble in an infinite medium, near a blank solid boundary, and above a hole in a solid boundary. We find in the case of the hole the unexpected formation of a counter jet that is directed away from the hole and into the bubble. These findings are contrasted to similar counter jetting behaviors from bubbles near boundaries with viscous and elastic properties.

INTRODUCTION

Cavitation refers to a wide range of processes by which bubbles (cavities) are formed within the body of a liquid, and to their non linear, large amplitude size oscillations [1,2]. Cavitation can be broadly categorized into gaseous or vaporous depending on the contents of the bubble interior. When a cavitation bubble oscillates in a infinite fluid medium, far away from boundaries and fluid interfaces, it normally does so symmetrically while retaining its spherical shape. However, when the cavitation bubble is bounded by a free surface interface or a solid boundary, for example, the bubble may not retain its spherical shape due to the asymmetry of the surrounding flow field. Jet-like formations are often observed in these cases and they are known as jets and counter jets. Asymmetry in the flow field can arise for multiple reasons such as in the presence of nearby bubbles, or when the effect of gravity (buoyancy) on the bubble is significant [3]. The generated jet will flow in a direction opposite to the gravitational vector. The asymmetrical flow field around a collapsing bubble can also be caused by the presence of a nearby solid surface. Upon bubble collapse, a fast, impulsive, re-entrant jet will form and it will be directed towards the solid surface as can be seen in **fig. 1a**.

Cavitation is very well known in liquid handling turbomachinery. Its occurrence is undesirable as it is associated with noise and vibrations, and, in extreme cases, with damage to solid surfaces such as blades and loss of machine performance.
One cause of cavitation pitting and damage to solid surfaces is widely believed to be the formation of re-entrant jets upon bubble collapse. The specific mechanism by which water jets cause damage is suspected to be the water hammer effect which scales with the liquid speed of sound [2].

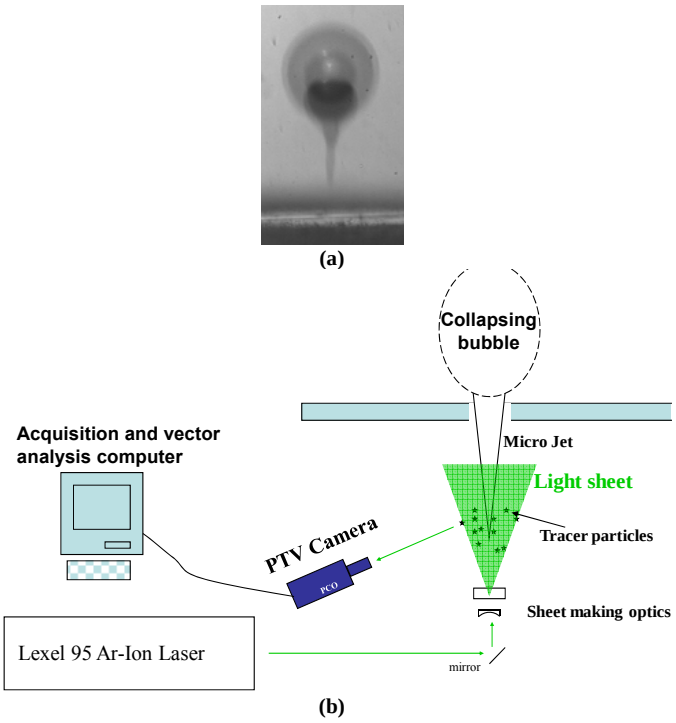

Fig. 1. (a) Picture depicting the jet formation near a *blank* solid boundary from a laser induced bubble. **(b)** Schematic of a micro jet forming above a hole in the boundary, with a flow visualization setup of the through hole jet.

If the wall-bounded bubble collapse can be engineered to control the impulsive micro-jet, then its deleterious effects may be channeled to useful applications such micro-surgery. The notion of using cavitation jetting in surgery has been used in ultrasonic studies where micro bubbles are driven by an acoustic field, e.g. from a high intensity focused ultrasound (HIFU), to oscillate violently and induce tissue impacting jets and surgical effects.

Water jets in theatre rooms are being generated by pressurized nozzles and used as a surgical cutting tool in a wide array of operations. The use of water jets as a cutting tool in precise surgeries has expanded over the last few years to cover a number of procedures. Examples of this include: cataract surgery [4], neurosurgery [5], renal surgery [6], bone prosthetic surgery [7], and liver resection [8]. The advantage of water micro-jets lies in the precise incisions they cause to soft tissue, while minimizing collateral damage to nearby cellular structures – mainly blood vessels. However, these pressure driven steady jets have some technical drawbacks such as clogging. The surgical performance of a jet may be improved if it were made unsteady and impulsive such as in the case of micro jets from cavitation bubbles.

In this work we are motivated by the micro jet formation from cavitation bubbles collapsing next to a solid boundary, their pitting effect on solid surfaces, and the potential for cultivating these jets for useful applications such as in micro surgery. It is hypothesized that if a small perforation (hole) is drilled in the solid boundary underneath the bubble where the jet is destined, then the jet may penetrate through this hole and be used in micro surgery at the outlet of the hole. See **Fig. 1b**. Such an idea has been also reported by the group of Professor Khoo [9,10]. The objective of this investigation is to provide a better understanding of the behavior of a single laser induced cavitation bubble when it collapses next to a solid boundary with a through hole underneath it, and the formation and behavior of the ensuing micro-jet.

NOMENCLATURE

t_c Bubble collapse time from inception to the point of minimum volume at first collapse

$R_{\max}$ Bubble maximum radius

τ_R : Rayleigh collapse time for a vaporous bubble

ΔP : Pressure difference between the bubble interior (vapor pressure of water at the liquid temperature) and the far away liquid

ρ : Liquid density

L : Distance from the wall to the bubble center

γ : Non dimensional distance from the center of the bubble to the boundary (normalized by the maximum bubble radius)

k : Collapse time prolongation factor for a non spherical bubble, equal to the collapse time of the non spherical deformed bubble normalized by the collapse time of a spherical bubble of equivalent radius. $k = \frac{t_{c,deformed}}{t_{c,spherical}}$

D_{hole} : Diameter of the through hole in the wall

α : Non-dimensional through hole diameter (normalized by the bubble maximum radius)

EXPERIMENTAL METHOD

In this study, single cavitation bubbles are generated in a water cuvette by focusing an infra red laser beam into a point in the liquid. A micro bubble grows at the focal point of the laser beam, expands to its maximum size, and then collapses to its minimum volume. The bubble may rebound once or more times after its initial collapse, and may disintegrate into many micro bubbles that are buoyed up to the surface of the water. The nominal size of the bubbles generated in this study is roughly a millimeter, with a life span of roughly a 100 micro seconds. Three experimental cases are studied: single bubbles in an infinite medium; single bubbles near a blank solid boundary; and single bubbles near a solid boundary with a perforated through hole. See **Fig. 2**.

Laser-induced bubble generation: The 6 mm laser beam from a Big Sky-Quantel pulsed Nd-YAG laser (120mJ max. energy per 6 nano second pulse) is passed through an optical train composed of three anti-reflection coated spherical lenses

of focal lengths (-30, +250, +75 mm). The optical train serves to expand the beam into a collimated diameter of 75 mm, and then focusing it at a fast angle onto a point near the center of the water cuvette. The steep focusing is required for a minimal Gaussian focal volume, where single clean bubbles can be generated repeatedly. The cuvette is a cube of 50 mm on the side made of clear cast acrylic, and is filled with drinking quality tap water. The water has enough micro impurities in it to absorb the laser energy and result in spherical bubble generation with almost every laser pulse. The generated bubbles were quite repeatable. The cuvette is placed on a translational stage allowing independent motion in the three orthogonal directions with micro-meter precision. This is needed to accurately distance the bubble position above the wall, and for accurate bubble centering with the through hole.

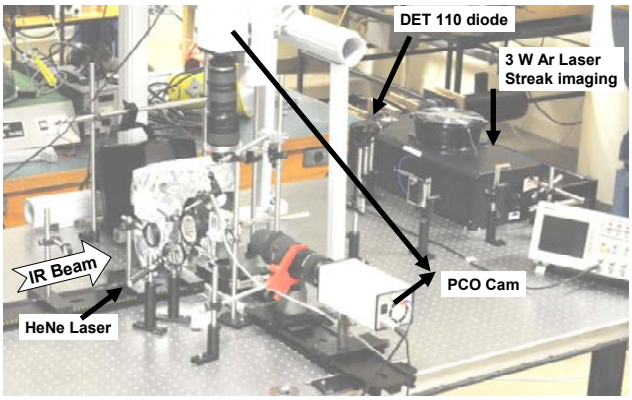

(a)

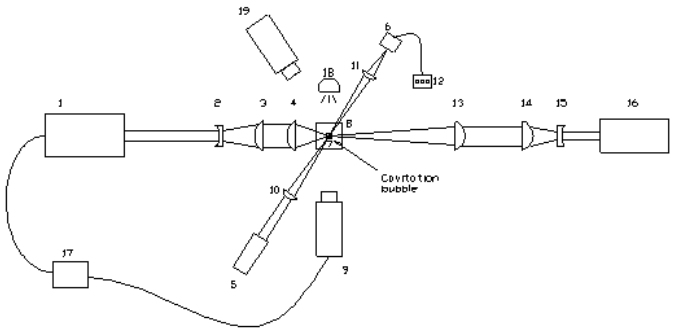

Fig. 2.b. Diagram of experimental setup. (1) Q-switched Nd: YAG laser (1064 nm wavelength, pulse duration 10 ns), (2) concave lens (f1 = 30 mm), (3) convex lens (f2 = 250 mm), (4) convex lens (f3 = 85 mm), (5) CW laser (650 nm, Power < 5mW), (6) High speed Si photo-detector 20 ns rise time, (7) brass target, (8) glass cuvette (45 x 45 x 50 mm), (9) fast shutter side view camera (PCO), (10) convex lens (f4 = 125 mm), (11) convex lens (f5 = 75 mm), (12) Oscilloscope digital storage 100 MHz, (13) convex lens (f6 = 400 mm), (14) convex lens (f7 = 250 mm), (15) concave lens (f8 = 9.7 mm), (16) CW Argon ion laser (Power 3 watt/ 457-514 nm wavelength), (17) Thorlabs timing box, (18) White light, (19) fast shutter top view camera (PCO).

(b)

Fig. 2. (a) A photograph of the actual experimental setup used to generate the cavitation bubbles (b) A schematic drawing of the setup with a detailed listing of the components.

The solid wall: In these studies the solid wall was a 2 cm square brass shim sheet of 200 microns thickness. The sheet was placed in the middle of the water cuvette, parallel to and underneath the IR beam path. The wall distance from the bubble was controlled accurately using the vertical translation stage. Drilling the micro perforations was done using the same pulsed IR beam underwater, but with the beam being normally incident and focused onto the brass sheet. Drilling a through hole normally takes a few hundred laser pulses at medium energy setting.

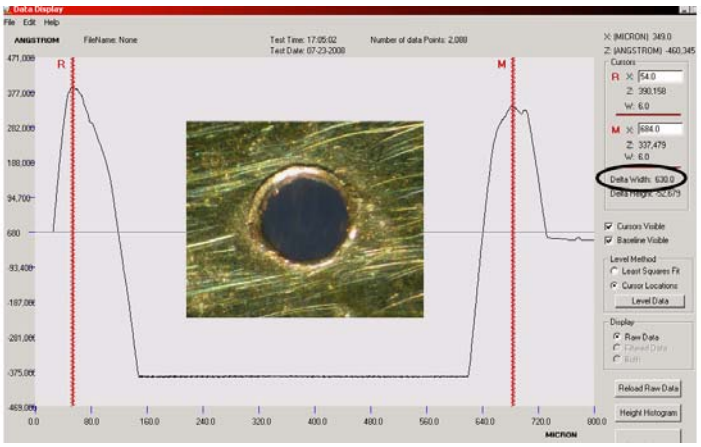

Fig. 3. A picture of a through orifice (625 microns in diameter) drilled in a brass sheet 0.2 mm thick by focusing the IR laser beam under water. Also shown is the profile-o-meter trace.

Fig. 3 shows an actual through hole with a 625 um diameter drilled by directly focusing the YAG laser energy onto the 0.2 mm thick brass sheet underwater. The hole was measured both using a profile-o-meter as shown, and using a scaled image of the magnified hole. Three hole diameters were investigated: 50, 200, and 625 microns.

Bubble tracing and imaging: The continuous time trace of the bubble volume history is recorded for each bubble using a Thorlabs DET 110 fast photo diode with 30 nano second rise time and a continuous wave red HeNe laser beam (635 nm). The red HeNe beam passes through the bubble inception point in the water cuvette and shines directly onto the photo diode's sensitive area. See **Fig. 2b**. When the incipient bubble grows and intercepts the red laser beam path, part of the beam energy is blocked from the photo receptor. The percentage of beam blockage is directly related to the bubble volume. Thus a continuous time trace of the bubble volume history is generated and could be viewed and recorded using a storage oscilloscope.

The bubble is also imaged using two fast shuttered single-frame, multi-exposure digital CCD camera (SensiCam-SVGA, PCO, Germany) with a 1280 by 1024 pixels resolution, and a 12 bit gray scale. Each camera is capable of acquiring up to 10 independent exposures on the same frame, and the exposure and the inter-exposure times can all be varied independently of each other down to half a micro second. The cameras are set to record orthogonal views of the bubble. The second camera is used to image the top view (i.e., the camera is set to image a plane parallel to the brass sheet) only in the case of the wall with a hole to guarantee that the bubble and the hole are co-

centered. White light illumination is used to improve the visualization. A hot mirror selectively filters out the infra-red beam and blocks it from entering the camera for protection from stray reflections.

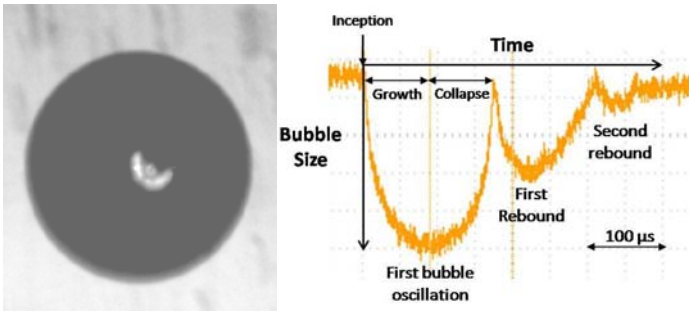

Fig. 4. A picture of a spherical bubble of 1.6 mm in diameter captured at its maximum expansion in an infinite medium; the camera exposure is 4 µs after a delay of 90 µs. The associated time trace of the bubble size time history as captured by the fast photo diode. After growing to its maximum size, the bubble collapses to its minimum size, and rebounds twice after that before it disappears.

Time reconstruction of the bubble shape history: Laser induced cavitation bubbles are known for their high repeatability and controllability. The bubbles generated in this study were also repeatable. By synchronizing the camera to the Q-Switch of the YAG laser and introducing controllable time delays, snapshots at different stages of the bubble life can be imaged, and time–tagged. By taking a large number of time-tagged image snapshots at various instances during the bubble life for bubbles that have the same volume-time-trace and the same maximum radius, we are able to sort theses images based on their time tag *a posteriori* and reconstruct the time history of the bubble shape. This has proven to be a useful tool in this study allowing imaging at effective frame rates on the order of a hundred thousand frames per second to be achieved at mega-pixel resolution without the need for more expensive high frame rate recordings.

Moreover, in addition to the image history reconstruction from multiple bubbles, we made use of the camera's multi-exposure, fast-shutter capability to provide further supporting information on the bubble behavior by taking multiple exposures for the same single bubble. We will be providing images of the bubbles using both approaches.

Visualization of the through flow underneath the hole: To verify the speed and the characteristics of the jet potentially penetrating to the other side of the hole, a particle streak imaging scheme was implemented beneath the hole in the solid wall. It consisted of the light beam from a 3-Watt Argon Ion Lexel laser that was formed into a thin laser sheet of approximately 50 microns thickness. The water was seeded with 100 nm titanium dioxide particles, and the particle reflections were recorded by the same PCO camera used to image the bubble above the hole. Using multiple exposures of different durations to generate the streaks, it was possible to deduce the flow velocity and direction underneath the hole.

RESULTS

Single bubbles generated in an infinite medium

Without a wall close by, the laser generated bubbles will grow and collapse in a symmetric manner, i.e., spherically. It is possible for the bubble to rebound after its initial collapse. But eventually the collapsing bubble will disintegrate into many micro bubbles that will buoy up to the surface of the water. **Fig. 4** shows a picture of the bubble captured at its maximum radius, with the oscilloscope time trace of the bubble volume history. The oscilloscope is triggered by the Q-Switch signal of the YAG laser. It is interesting to note in this example that the bubble initially collapses to a finite non-zero volume, which may be due to the presence of non condensable gases present in the bubble interior.

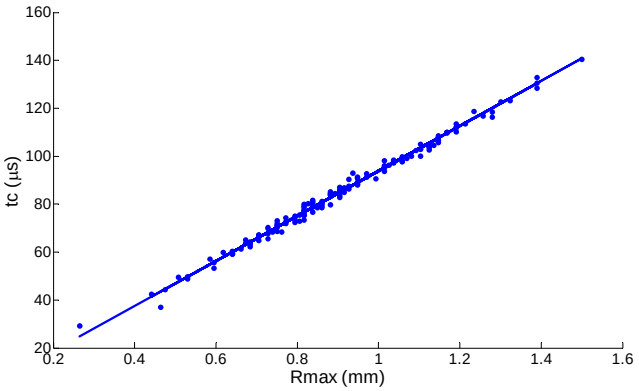

Fig. 5. Scatter plot of the bubble collapse time with its maximum radius. Also shown is a line depicting twice the Rayleigh time ($2\tau_R$).

Fig. 5 shows a scatter plot of the bubble life span (t_c) (time from inception to first collapse) against the bubble maximum radius for bubbles ranging in maximum radius from 0.4 to 1.5 mm. The bubble radius was directly measured from the scaled camera images taken at the point of maximum bubble expansion, while the life span of the bubble was measured from the time trace provided by the fast photo diode. Also shown on the same plot is the Rayleigh line for spherically collapsing vapor bubbles. The Rayleigh collapse time (τ_R) for a bubble of maximum radius (R_{max}) is given by [1]: $\tau_R = 0.915 R_{max}\sqrt{\rho/\Delta P}$, where: ΔP is the pressure difference between the bubble interior (water vapor pressure at the liquid temperature) and the far away liquid, and ρ is the liquid density. Here, ΔP is 97 kPa, with the vapor pressure taken at the water temperature. The generated bubbles follow closely the Rayleigh scaling for the collapse time. This is expected, since laser induced bubbles are mostly vaporous. Additionally, the scatter in the data is not significant indicating that the bubbles are repeatable.

Single bubbles generated above a blank solid boundary (no hole)

Introducing a solid surface close to the cavitation bubble will disturb the symmetry of the flow field, and will cause the bubble shape to deviate from the spherical shape. A micro jet directed towards the solid boundary will form, and it starts by penetrating the top surface of the bubble, and continues in the direction of the solid boundary after it has punctured through the lower bubble surface. The dynamics of the jet depend on the dimensionless distance $\gamma = \frac{L}{R_{\max}}$, with L being the distance from the center of the bubble to the wall. The wall-directed jet forms as the bubble approaches a dimensionless distance γ of around 3 to 4 from the wall, in the absence of tangible buoyancy effects, which is the case here with the small bubbles.

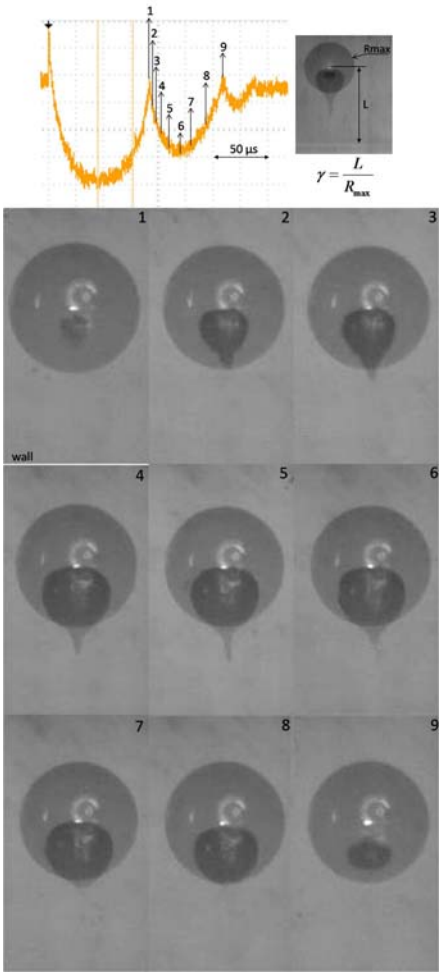

Fig. 6. A time-reconstruction of the bubble shape history when it collapses next to a blank solid boundary with $\gamma = 2.2$. Each frame has two exposures. One exposure of 3 µs is always taken when the bubble is at its maximum radius (Rmax=1.65 mm). The other exposure of 6 µs is timed to capture the bubble progress starting at its initial rebound after the first collapse.

Fig. 6 provides a brief depiction of the events leading to jet formation. The upper right figure shows three superposed exposures of the same bubble at $\gamma = 2.2$. The first exposure shows the spherical bubble at its maximum radius. The second exposure shows the bubble near the point of minimum expansion toward the end of the first collapse (dark pan-cake shaped spot in the center of the image). A counter jet formation away from the wall can be seen in zoomed views (e.g. **Fig. 7**), indicating the start of the bubble deviation from sphericity. The third exposure is taken when the bubble has rebounded to its new maximum expansion with a clear jet-formation directed towards the wall. The jet forms during the rebound phase as the bubble translates closer to the solid boundary. This figure also focuses on the rebound phase of a bubble near a blank solid boundary ($\gamma = 2.2$) to provide more details on the jet formation details seen in the preceding figure. It is reconstructed from multiple bubbles of the same life span, maximum radius, time trace, and distance to the wall. Each of the frames shows two superposed exposures: the first is taken when the bubble is at its maximum radius, and the second depicts the bubble at a preset delay after its first collapse. The wall-directed jet is observed right after the bubble starts its first rebound phase. The jet achieves its maximum extension in the direction of the solid boundary near the point of maximum rebounded bubble size. As the bubble starts to contract again, the jet *retracts* from the wall. The bubble collapses to a minimum size again.

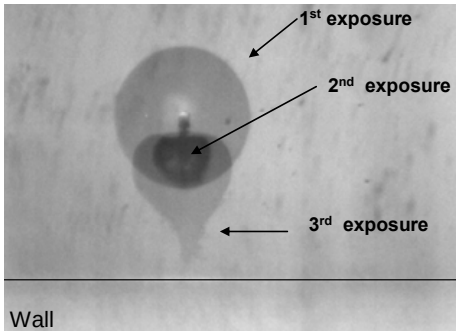

Fig. 7. A laser induced cavitation bubble collapsing near a solid surface with γ=2.2. Three exposures are taken at three different times. The first 3 µs-long exposure is triggered 102 µs) after the bubble inception, at the point of maximum radius (0.85 mm). The second 3-µs long exposure is triggered just after the bubble reaches its minimum size. A counter micro-jet can be seen clearly. The third 3 µs exposure is triggered during the bubble rebound phase (t=183 µs) when the bubble is at its new (rebounded) maximum expansion, and it clearly shows a main micro jet that appears to be traveling to the solid surface.

Fig. 6 suggest that the "jet" in this case (γ above ~ 1.8) is mostly a shape deformation of the rebounding (growing) bubble rather than a thrust of surrounding liquid water accelerating toward a collapsing bubble – the bubble growing around the deformation. This will help in understanding the behavior of a bubble collapsing in the presence of a through hole in the boundary.

It was possible to analyze the multi-exposed images of the jet to infer the velocity of the jet tip. See **Fig. 7**. The inter-exposure time separation during the study of the jet velocity was set at 3 μs. **Fig. 8** shows that the jet tip velocity as a function of time after the first bubble collapse (initiation of first bubble rebound) for multiple ranges of distance from the wall γ. The tip velocity is at its maximum right after the start of the rebound and it decreases as it moves toward the wall. The maximum tip velocity within the observed time frame is relatively small and is less than 50 m/s.

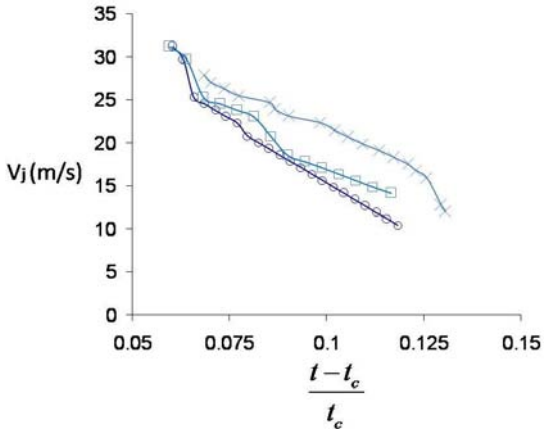

Fig. 8. Jet tip velocity for multiple ranges of distance from the wall, γ. Three ranges of γ are presented. The data corresponding to the range $1.82 < \gamma < 2.02$ are shown in (x); those corresponding to the range $2.38 < \gamma < 2.58$ are shown in large squares (□), and (○) for the range $2.55 < \gamma < 2.815$.

For smaller values of γ the effect of the wall on the bubble becomes stronger. The bubble can deform greatly during its growth phase. For example, in the bubble shown in **Fig. 9** ($\gamma \approx 1$), the lower bubble wall is nearly flattened by the solid boundary when the bubble is near its maximum size.

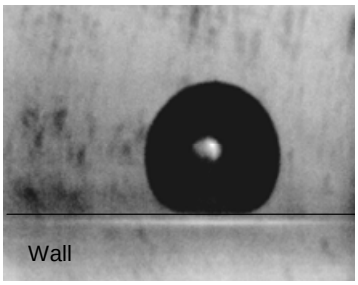

Fig. 9. A laser induced cavitation bubble collapsing near a solid surface with γ=1. One exposure of 3 μs of the bubble is taken for this case to show the bubble at its maximum volume (R_{max}= 0.9 mm). The bubble is not spherical anymore, but is flattened at the bottom by the solid wall.

We also estimate the collapse time prolongation factor (k) of a bubble generated next to a solid boundary which is a measure of the retardation of the velocity of the bubble wall when compared with a spherical bubble of equivalent size, **Fig. 10**.

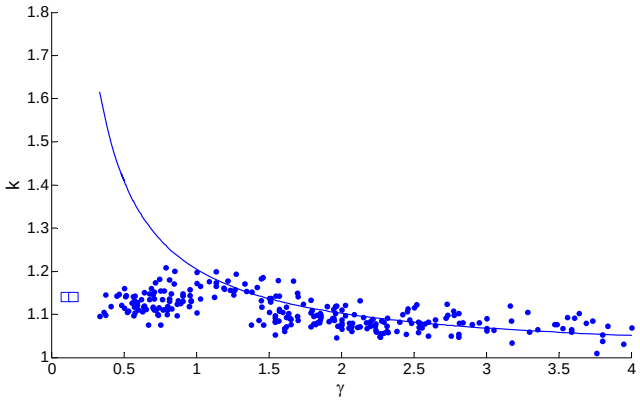

Fig. 10. Collapse time prolongation factor. The experimental data are shown in dots and are compared to the Rattray computed ***k***–line [11] for the same distance γ. Also shown (two open squares) are the Godwin [12] results for very small γ.

An unbounded bubble in an infinite medium has a prolongation factor of $k = 1$. The retardation factor increases as the bubble normalized distance from the wall decreases. The data compare well to those of Rattray [11] and Godwin *et al.* [12].

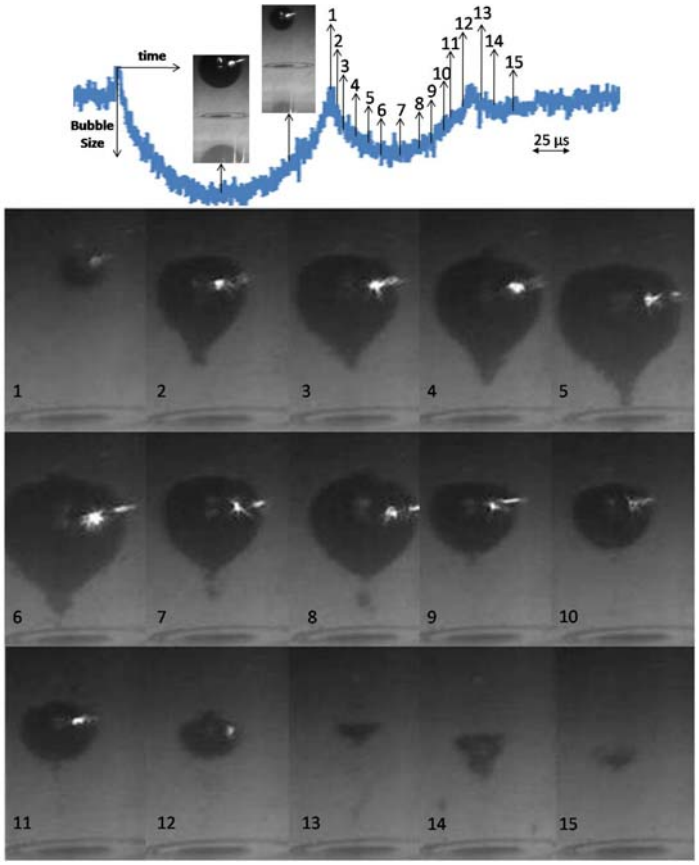

Fig. 11. A history reconstruction of the bubble shape (R_{max}=0.81 mm) when collapsing next to a solid wall with a 720 microns hole [γ=2.27, α=0.87] beyond the initiation of the first rebound. A reflection of the bubble can be seen

off the wall. The frame numbers correspond to the marked points on the time trace.

Single bubbles generated above a solid boundary with a through hole

It is expected that the bubble behavior in the presence of the hole in the wall will depend on the normalized distance of the bubble from the wall γ and on the normalized hole diameter α, with $\alpha = \frac{D_{hole}}{R_{\max}}$. In the limit that the normalized hole diameter α goes to zero this will render the solid wall case, while the infinite medium case corresponds to an infinite α.

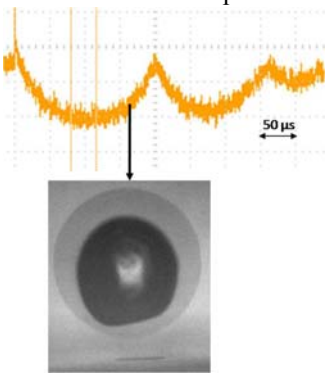

Fig. 12. For the case of γ=1.46 and α=0.7, this figure shows a frame with two exposures of the same bubble. The first exposure of 1 µs is at the point of maximum expansion (R_{max}=0.9 mm), while the second of 6 µs is taken a short while afterwards, during the bubble implosion phase. (D_{hole}=625 microns).

Fig. 11 shows a reconstruction of the shape history of a bubble neighboring a solid boundary with a hole of diameter 625 microns. The bubble shape history is shown starting near its point of minimum radius after the first collapse and its initial rebound. For this wall separation distance $\gamma = 2.27$ and $\alpha = 0.87$, the bubble behaves in a very similar way to the solid wall case, as if the hole effect is almost absent. One can compare this case with the blank wall one shown in **Fig. 6**. A similar behavior could be seen as the normalized distance to the wall is further reduced.

As the bubble gets closer to the hole, it can slightly bulge out towards the hole. The bubble becomes slightly non-spherical at maximum expansion and the effect of the slight bulging becomes pronounced as the bubble contracts. **Fig. 12** shows this behavior for a single bubble of $\gamma = 1.46$ and $\alpha = 0.7$ using two camera exposures; the first exposure of 1 µs is at the bubble maximum expansion, while the second of 6 µs is taken a short while afterwards, during the bubble implosion phase. This bulging towards the hole can result in a bubble pinch-off as will be seen below.

Fig. 13 shows a reconstructed image sequence of a bubble generated at $\gamma = 1.13$ and $\alpha = 0.65$. The bulging towards the hole, as well as a pinch off of a secondary bubble can be seen.

Moreover, the top bubble wall collapses faster that the bottom bubble wall. The center of the bubble moves towards the wall as it proceeds through the collapse process. Observation of bubbles forming slightly off the center of the hole provides clearer evidence of the bubble-pinching effect by the hole as seen in **fig. 14** for the case of $\gamma = 1.04$ and $\alpha = 0.59$. It shows a vapor bridge between the lower wall of the main bubble, and the hole. Once the pinch-off process is completed and two separate bubbles transpire, a counter micro jet develops, penetrating the lower wall of the main bubble near the pinch-off point. The jet is directed upwards towards the main bubble center as shown in subsequent figures.

Fig. 15 is an image sequence reconstruction for the case of $\gamma = 0.94$ and $\alpha = 0.63$. A secondary bubble splits from the main bubble and stays near the hole which later becomes pancaked as the main bubble collapses.

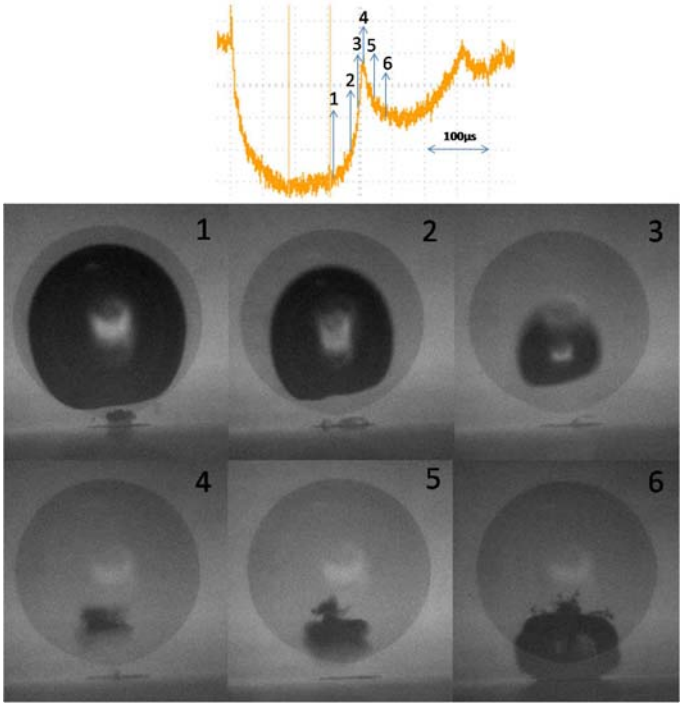

Fig. 13. A reconstructed image sequence of a bubble (R_{max}=0.96 mm) generated at $\gamma = 1.13$ and $\alpha = 0.65$. The bulging towards the hole (D_{hole}=625 microns), as well as the pinch off can be seen. Two exposures are taken in each frame: the first of 1 µs is always at the maximum expansion while the second of 5 µs corresponds to a number on the bubble time trace. 15 µs is the delay between two consecutive frames.

Meanwhile, a counter micro jet is seen to be directed upwards to the center of the main bubble, coming from the lower wall of the main bubble. The bubble stays attached to the wall as it collapses to its minimum size.

The counter jet can become strong enough to penetrate the upper bubble wall as γ decreases. Shown in **Fig. 16** is an image sequence reconstruction of the bubble and jet behavior for the case of $\gamma = 0.6$ and $\alpha = 0.63$. Each frame shows two exposure of the bubble: the first captures the bubble at its maximum

radius, and the second at progressing delays from the point of inception. The remnants of the completely collapsed bubble and the collapsed gas pocket entrained in the counter jet are seen.

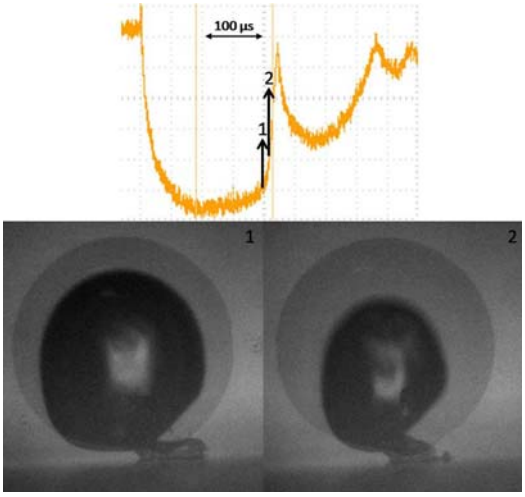

Fig. 14. For the case of γ=1.04 and α=0.59, this figure shows two frames with two exposures of a 1.05 mm maximum radius bubble. For the two frames, the first exposure of 1 µs is at the point of maximum expansion, while the second of 5 µs is taken a short while afterwards, during the bubble implosion phase. (D_{hole}=625 microns).

Fig. 17 focuses on the collapse phase of a bubble generated at a similar wall distance to the case shown in **Fig. 16** but for a smaller normalized hole diameter $\alpha = 0.06$, with the normalized distance from the wall kept constant, $\gamma = 0.6$. The bubble shape, and counter jet formation are quite similar to the larger-hole case.

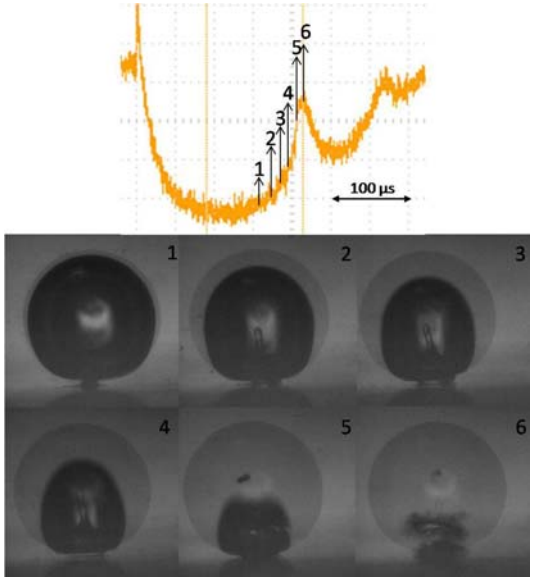

Figure 15. A reconstruction of the bubble history as it collapses from the point of its maximum expansion with $\gamma = 0.94$ and $\alpha = 0.625$. Two exposures are shown on each frame. The first of 1 µs is taken at the maximum bubble size (R_{max}=1 mm), while the other exposure of 5 µs at progressing delays from that point. (D_{hole}=625 microns).

The flow behavior underneath the hole was observed for the case of $\gamma = 0.55$ and $\alpha = 0.07$ using sheet illumination and micro particles for flow tracing, **Fig. 18**.

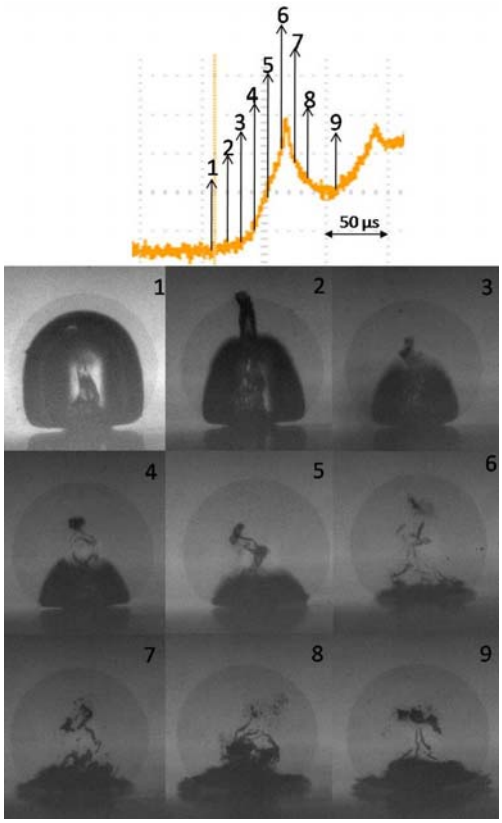

Fig. 16. A reconstruction of the bubble history as it collapses from a point after its maximum expansion with $\gamma = 0.6$ and $\alpha = 0.63$. Two exposures are shown on each frame. The first of 1 µs is taken at the maximum bubble size (R_{max}= 0.98 mm), while the other exposure of 5 µs at progressing delays from that point. (D_{hole}=625 microns).

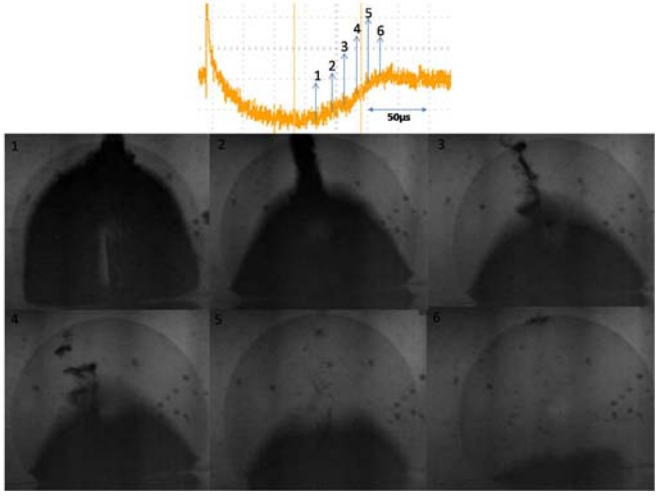

Fig. 17. The collapse phase of a bubble generated at a similar wall distance to the case shown in Fig. 18 but for a much smaller hole diameter (D_{hole}=50 microns), with $\gamma = 0.6$ and $\alpha = 0.06$. No rebound was detected!

Analysis of the tracer particles velocities indicates that as the bubble grows after inception a downward flow through the hole is generated with speeds of ~ 4 m/s, but after the bubble has reached its maximum volume and proceeds to collapse the flow beneath the hole is now directed upward towards the hole. This is consistent with the counter-jet formation shown in this figure and more clearly in the previous figures.

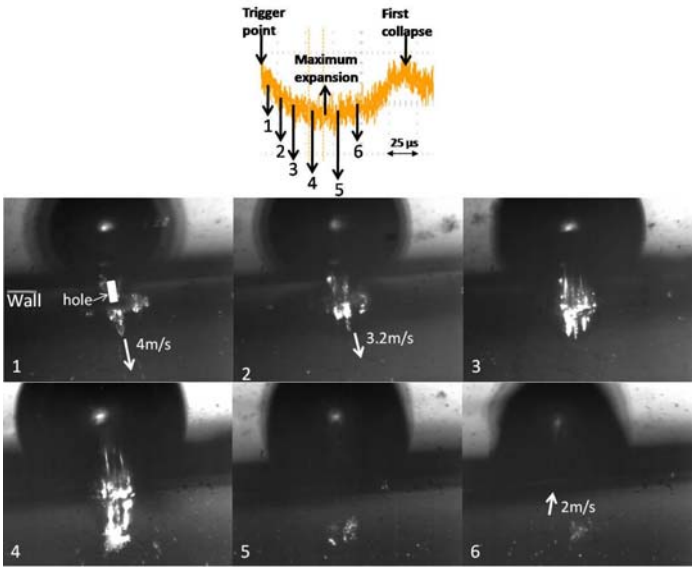

Fig. 18. Flow behavior underneath the hole (D_{hole}=50 microns) observed using light sheet illumination for the case of $\gamma = 0.55$ and $\alpha = 0.07$ (Rmax= 0.7 mm).

DISCUSSION & CONCLUSIONS

Wall-directed micro-jet formation from cavitation bubbles collapsing near boundaries is believed to be one mode of damage to solid surfaces, and a cause for sonoporation of tissue in ultrasound contrast agent insonification treatments. We studied the dynamics of a laser induced bubble in an infinite medium and near a solid boundary. The data collected in both cases match well with data reported in the literature [13]. We further studied the single bubble collapse over a through hole in a solid boundary. We found that the formation of the micro-jet from the collapsing bubble was directed away from the hole and the wall. This counter jet formation did not exist in the case of the blank wall and it bears resemblance to bubble behavior in therapeutic ultrasound treatments; in particular, the studies of Brujan *et al.* [15] and Chen *et al.* [16]. In the former, the researchers presented high speed images of laser induced cavitation bubbles near a solid elastic boundary for various elasticity moduli. They found that the jet formation was directed towards the solid boundary except for a narrow range of elasticity moduli when the jet was directed away from the solid boundary. In the other study, Chen *et al*. used a high intensity ultrasound transducer to drive micro-bubble contrast agents injected into the micro-blood vessels of a rat *ex-vivo*. They found that the collapsing bubble produced a micro-jet that was directed away from the vessel wall pulling some of the tissue with it into the bubble in a process they termed invagination.

The counter jet formations in these studies, though of different experimental nature particularly the visco-elastic boundary effects, bear resemblance with the counter jetting from a hole in a rigid boundary.

Thus it seems that both modes of jetting and counter jetting are possible in cavitation bubbles near boundaries. Ohl *et al.* [17] provided a summary of the effects of boundary density and boundary elasticity on the bubble behavior, and reported a third scenario in which the bubble can disintegrate into smaller bubbles. Blake and Gibson [18] and Blake and Cerone [19] considered the case of a cavitation bubble near the interface between two fluids of dissimilar densities, and their analysis suggested that the jet formation would be directed towards the denser fluid. A spherical bubble model near tissue implemented by Freund [20] and taking into account real tissue viscosity and elasticity suggested that tissue viscosity is a critical factor in affecting the dynamics of the bounded bubble. Thus both modes of jet formation (towards, and away from the boundary) were found to be possible, while it was not very obvious why one mode would appear and not the other in a specific situation. Our results provide additional evidence on the jetting behavior near a modified boundary (rigid wall with a hole). Similar studies were conducted by the group of Prof. BC Khoo [21, 22, 23], in which spark-generated single bubbles were allowed to collapse above a hole drilled in a solid boundary. These studies showed very interesting bubble behaviors, but did not show the counter jetting behavior we present here and this may be due to many differences present between our studies. For instance, our bubbles are significantly smaller in size, and they are non-intrusively introduced into the liquid (pulsed laser) where no wire electrodes need to be present near the bubble.

It is thus concluded that predicting the behavior of the jet formation with a modified rigid boundary (modified by a hole) may not be straight forward contrary to what was initially hypothesized in the onset of the study.

ACKNOWLEDGMENTS

Funding for this work was provided by the Arab Science and Technology Foundation (ASTF), project HE06160. The major equipment was acquired through a grant from the American Schools and Hospitals Abroad (ASHA).

REFERENCES

1. Brennen 1995, "*Cavitation and Bubble Dynamics,*", Oxford University Press, NY
2. Franc JP, Avellan F, Belhadji B *et al.*, 1995, "*La Cavitation: Mecanismes Physiques et Aspects Industriels*", Presses Universitaires de Grenoble

3. R. Blake and D. C. Gibson, 1987, ‘‘Cavitation bubbles near boundaries,’’ Annu. Rev. Fluid Mech. **19**, pp 99–123.
4. Wilhelm FH, Holtkamp A, Theurer A, Darman J jr., Duncker G, and Wilhelm L, “Examination of resistance of the lens capsule against the waterjet,”, *Ophthalmologe*, **96**, pp. 640-642
5. Kodama T, Takayama K, and Uenohara H, 1997, “A new technology for revascularization of cerebral embolism using liquid jet impact,” *Phys. Med. Biol.*, **42**, pp. 2355-2367
6. Miller JM, Palancker DV, Vankov A, Marmor MF, and Blumenkranz MS, 2003, “Precision and safety of the pulsed electron avalanche knife in vitreoretinal surgery,” *Arch. Ophthalmol*, **121**(6), pp 871-877
7. Honl M, Rentzsch R, Schwieger K, Carrero V, Dierk O., Dries S, Louis H, Pude F, Bishop N, Hille E, and Morlock M, 2003, “The water jet as a new tool for endoprosthesis revision surgery – An *in-vitro* study on human bone and bone cement,” *Biomed. Mater. & Eng.*, **13**, pp 317-325
8. Rau HG, Meyer G, Cohnert TU, Schardey HM, Jauch K, and Schildberg FW, 1995, “Laparoscopic liver resection with the water jet dissector,” *Surg. Endosc.*, 1995(9), pp. 1009-1012
9. Khoo BC, Klaseboer E, and Hung KC, 2005, “A collapsing bubble-induced micro-pump using the jetting effect”, *Sensors & Actuators*, **118**, pp 152-161
10. Lew KSF, Klaseboer E, and Khoo BC, 2006, “ A collapsing bubble-induced micropump: an experimental study,” *Sensors & Actuators A: Phys*
11. M Rattray Jr, “Perturbation Effects in Cavitation Bubble Dynamics,” Ph.D Thesis, California Institute of Technology, 1951
12. Godwin RP, Chapyak EJ, Noack J, and Vogel A, “Aspherical bubble dynamics and oscillation times,” Proc. SPIE, **3601**(225), 1999
13. Vogel A, Lauterborn W, and Timm R, “Optical and acoustic investigations of the dynamics of laser-produced cavitation bubbles near a solid boundary”, *J. Fluid Mech.* **206**, pp299, 1988
14. Prentice P, Cuschieri A, Dholakia K, Prausnitz M, and Campbell P, “Membrane disruption by optically controlled microbubble cavitation,” *Nature Physics*, **1**, pp 107, 2005
15. Brujan EA, Nahen E, Schmidt P, and Vogel A, “Dynamics of laser-induced cavitation bubbles near an elastic boundary,” *J. Fluid Mech.* **433**, pp. 251, 2001
16. Chen H, Brayman AA, Bailey MR, and Matula TJ, “Direct observation of microbubble interactions with ex vivo microvessels,” *J. Acoust. Soc. Am.* **125**(4) pp. 2680, 2009
17. Ohl SW, Klaseboer E, and Khoo BC, “The dynamics of a non-equilibrium bubble near bio-materials,” *Phys. Med. Biol.*, **54**, pp6313-6336, 2009.
18. Blake JR and Gibson DC, “Cavitation bubbles near boundaries,” *Ann. Rev. Fluid Mech*, **19**, pp.99-123, 1987
19. Blake JR and Cerone P, “A note on the impulse due to a vapor bubble near a boundary,” *J. Aust. Math. Society B*, **23**, pp383, 1982
20. Freund JB, “Suppression of shocked-bubble expansion due to tissue confinement with application to shock-wave lithotripsy,”, *J. Acoustical Soc. Am.*, **123**(5), pp2867, 2008
21. Lew K, Klaseboer E, and Khoo BC, “A collapsing bubble-induced micropump: An experimental study,” *Sensors and Actuators A*, **133**, pp 161, 2007
22. Pavard D, Klaseboer E, Ohl SW, and Khoo BC, “Removal of particles from holes in submerged plates with oscillating bubbles,” *Phys. Fluids*, **21**, Art. No 083304, 2009
23. Khoo BC, Klaseboer E, and Hung KC, “A collapsing bubble-induced micro-pump using the jetting effect,” *Sensors & Actuators: A. Physical*, **118**(1), pp152, 2005